

Dynamically dominant excitations of string solutions in the spin-1/2 antiferromagnetic Heisenberg chain in magnetic fields

Masanori Kohno

WPI Center for Materials Nanoarchitectonics, National Institute for Materials Science, Tsukuba 305-0047, Japan

(Dated: February 3, 2022)

Using Bethe-ansatz solutions, we uncover a well-defined continuum in dynamical structure factor $S^{+-}(k, \omega)$ of the spin-1/2 antiferromagnetic Heisenberg chain in magnetic fields. It comes from string solutions which continuously connect the mode of the lowest-energy excitations in the zero-field limit and that of bound states of overturned spins from the ferromagnetic state near the saturation field. We confirm the relevance to real materials through comparisons with experimental results.

PACS numbers: 75.10.Jm, 75.40.Gb, 75.50.Ee

The spin-1/2 antiferromagnetic Heisenberg chain exhibits intriguing quantum many-body effects, associated with modern concepts in condensed-matter physics, such as spin liquids, quantum criticality and fractionalization. Also, this system is an excellent platform to make precise comparisons between experiments and theories: Various intriguing features predicted by exact solutions [1] can be confirmed by accurate experiments on quasi-one-dimensional materials. Actually, it is established that dynamical properties in the absence of magnetic field are characterized by quasiparticles called spinons [2, 3] through precise comparisons between theoretical predictions and experimental results [4, 5, 6].

In magnetic fields, dynamical properties are more complicated. Some basic features of dominant excitation spectra can be understood by modifying the 2-spinon continuum in zero field according to the strength of magnetic fields in the k - ω plane [7, 8, 9]. The distributions of spectral weights in $S^{+-}(k, \omega)$ and $S^{zz}(k, \omega)$ are effectively expressed by low-order particle-hole excitations in Bethe-ansatz solutions [9, 10, 11]: The dominant excitations in $S^{+-}(k, \omega)$ and $S^{zz}(k, \omega)$ are known as 2-psinon (2ψ) excitations and psinon-antipsinon ($\psi\psi^*$) excitations, respectively [10, 11]. Their properties have been investigated in detail by using Bethe-ansatz solutions [10, 11, 12, 13, 14, 15, 16, 17, 18, 19].

As for $S^{+-}(k, \omega)$, the situation is much more complicated. Except the low-energy modes near momentum $k=0$ [9, 10, 18, 19, 20] and $k=\pi$ [9, 10, 19, 20], behaviors of $S^{+-}(k, \omega)$ have not been clarified: In Ref. [9], the continuum of $\psi\psi^*$ excitations was predicted to persist in the thermodynamic limit based on the classification by the Bethe formalism. However, numerical results indicated that the spectral weight in the $\psi\psi^*$ continuum is rather small except near the edges, and there exists a large fraction of spectral weights above the continuum [9, 20].

In this Letter, mainly focusing attention on behaviors of $S^{+-}(k, \omega)$ in magnetic fields, we identify excitations having large spectral weights to clarify overall dynamical features of the Heisenberg chain in magnetic fields.

We consider the spin-1/2 antiferromagnetic Heisenberg

chain with L sites, M down spins ($M \leq L/2$) and periodic boundary conditions. The Hamiltonian is defined as

$$\mathcal{H} = J \sum_{x=1}^L \mathbf{S}_x \cdot \mathbf{S}_{x+1} - HS^z, \quad (1)$$

where \mathbf{S}_x is the spin-1/2 operator at site x , and $J > 0$. Magnetic field H at $S^z/L = 1/2 - M/L$ in the thermodynamic limit is obtained in Ref. [21]. In the Bethe ansatz [1], the wave function, energy and momentum of an eigenstate are expressed by a set of rapidities $\{\Lambda_j\}$ which is obtained from the Bethe equation: $L \arctan(\Lambda_j) = \pi I_j + \sum_{l=1}^M \arctan[(\Lambda_j - \Lambda_l)/2]$, once a set of $\{I_j\}$ is given. Here, I_j ($j=1 \sim M$) are called Bethe quantum numbers, which are integers (half-odd integers) within $|I_j| \leq (L-M-1)/2$ for odd (even) $L-M$ as in Fig. 1 (a-e) for solutions of real $\{\Lambda_j\}$. Distributions of $\{I_j\}$ are somewhat analogous to momentum distributions of spinless fermions. As in Fig. 1 (b), a hole (particle) created inside (outside) the $\{I_j\}$ of the ground state is called psinon (antipsinon) and denoted by ψ (ψ^*) [10, 11].

It is also known that there are solutions with complex rapidities [1]. Later, we will consider solutions with an n -string ($n \geq 2$), i.e. a set of n rapidities expressed as $\Lambda_j = \bar{\Lambda} + i(n+1-2j) + i\eta_j$ for $j=1 \sim n$, where $\bar{\Lambda}$ is real, and $\eta_j = O(e^{-cL})$ with $c > 0$ [1, 16, 22, 23]. We take real Λ_j for $j \geq n+1$, and denote the n -string solutions by S_n . These solutions are specified by two sets of $\{I_j\}$ [22]: One is for the real rapidities, and the other is for the n -string, which we denote by $\{I_j^r\}$ and $\{I_j^i\}$, respectively. For S_n ($n \geq 2$), $\{I_j^i\} = I_1^i$, $|I_1^i| \leq L/2 - M$ as in Fig. 1 (f-2). We denote ψ and ψ^* of $\{I_j^r\}$ by ψ_s and ψ_s^* , respectively, and regard $\{I_j^i\}$ without ψ_s or ψ_s^* also as a part of those with $\psi_s \psi_s^*$.

We investigate behaviors of dynamical structure factors defined as $S^{\bar{\alpha}\alpha}(k, \omega) = \sum_i M^{\bar{\alpha}\alpha}(k, \epsilon_k^i) \delta(\omega - \epsilon_k^i)$ for $\alpha = -, +$ and z . Here, $M^{\bar{\alpha}\alpha}(k, \epsilon_k^i)$ is the transition rate between the ground state $|\text{G.S.}\rangle$ in a magnetic field and an excited state $|k, \epsilon_k^i\rangle$ with excitation energy ϵ_k^i and momentum k , defined as $M^{\bar{\alpha}\alpha}(k, \epsilon_k^i) = |\langle k, \epsilon_k^i | S_k^\alpha | \text{G.S.} \rangle|^2$. We calculated $M^{\bar{\alpha}\alpha}(k, \epsilon_k^i)$ of the Heisenberg chain, following Refs. [15, 16, 17, 18, 23, 24] where $M^{\bar{\alpha}\alpha}(k, \epsilon_k^i)$ is expressed in a determinant form whose matrix elements are

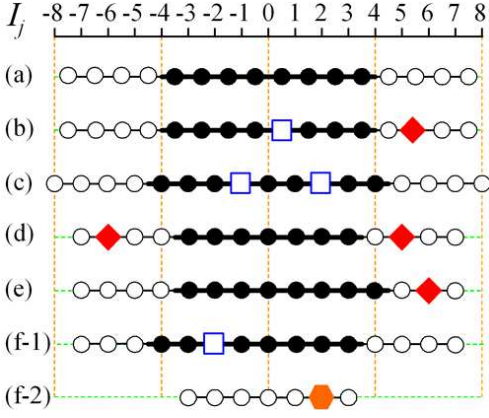


FIG. 1: Distributions of Bethe quantum numbers $\{I_j\}$. Filled symbols denote $\{I_j\}$ of the ground state of $M=8$ and typical excited states in dynamical structure factors for $0 \leq k \leq \pi$ in $L=24$. Blue open square and red solid diamond denote psinon (ψ) and antipsinon (ψ^*) [10], which are located at points on thick and thin lines, respectively. (a) Ground state. (b) $\psi\psi^*$ for $S^{zz}(k, \omega)$. (c) 2ψ for $S^{+-}(k, \omega)$. (d) $2\psi^*$ for the continuum near $k=\pi$ in $S^{+-}(k, \omega)$. (e) $1\psi^*$ for the low-energy mode near $k=0$ in $S^{+-}(k, \omega)$. (f-1) 1ψ of $\{I_j^i\}$ for 2-string solutions in $S^{+-}(k, \omega)$. (f-2) I_1^i for the n -string of S_n ($n \geq 2$) in $S^{+-}(k, \omega)$.

expressed in terms of rapidities [24]. As for string solutions with an n -string ($n \geq 2$), we calculated $M^{\bar{\alpha}\alpha}(k, \epsilon_k^i)$ after transforming the matrices so that singularities in determinants can be cancelled as in Refs. [16, 23]. In $S^{+-}(k=0, \omega)$, we took into account the resonant mode of the field-induced magnetization [9, 10, 18, 19, 20]. In this Letter, we show results on dynamical structure factors in units of $1/J$ for $0 \leq k \leq \pi$, noting $S^{\bar{\alpha}\alpha}(k, \omega) = S^{\bar{\alpha}\alpha}(-k, \omega)$, $\alpha = -, +$ and z .

We calculated the spectral weight in $L=320$, using up to $2\psi 2\psi^*$ excitations, and evaluated the contributions to sum rules [25]. The results are shown by open symbols in Fig. 2 (a) and (b). The spectral weight of up to $2\psi 2\psi^*$ excitations in $S^{+-}(k, \omega)$ satisfies more than 90% of the sum rule in $L=320$ as shown by open diamonds in Fig. 2 (b). The spectral weight in $S^{+-}(k, \omega)$ severely decreases in the small S^z regime as shown by open circles in Fig. 2 (a). Figure 2 (e) shows $S^{+-}(k, \omega)$ in the small S^z regime. Although $S^{+-}(k, \omega)$ should be continuously connected to that in zero field (Fig. 2 (d)) as the magnetic field decreases, most of the spectral weight in $S^{+-}(k, \omega)$ is missing. In particular, the large intensity near the des Cloiseaux-Pearson mode (dCP) [26] (the lower edge of the continuum in zero field) is almost lost. This implies that there are other important excitations for $S^{+-}(k, \omega)$.

To explain the origin of the missing spectral weight, we consider S2 and S3 defined above. Among many states in S2 and S3, we found that S2 with $\psi_s \psi_s^*$ and S3 with $2\psi_s$ have large weights in $S^{+-}(k, \omega)$. By taking into account these string solutions, $S^{+-}(k, \omega)$ in the small S^z regime almost recovers the missing weight near the dCP

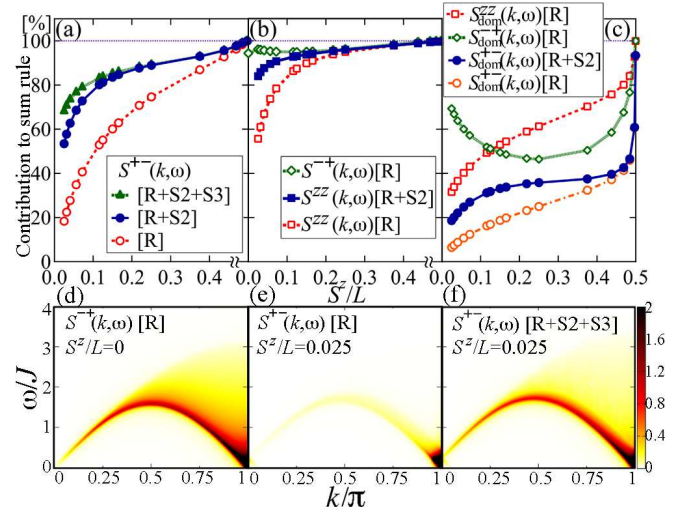


FIG. 2: (a,b) Contributions to sum rules from solutions of up to $2\psi 2\psi^*$, string solutions with a 2-string and those with a 3-string, denoted by R, S2 and S3, respectively, in $L=320$ for (a) $S^{+-}(k, \omega)$, (b) $S^{-+}(k, \omega)$ and $S^{zz}(k, \omega)$. (c) Contributions of dynamically dominant excitations in $L=2240$. (d) $S^{+-}(k, \omega)$ in zero field. (e,f) $S^{+-}(k, \omega)$ at $S^z/L=0.025$ without and with the contributions of S2 and S3. In (d-f), the data obtained in $L=320$ are broadened in a Lorentzian form with full-width at half maximum (FWHM) $0.08J$. For S2 and S3 in (a,b,f), we took the $O(L^3)$ states described in the text.

mode and that of the continuum near $k=\pi$ as shown in Fig. 2 (f). The intensity near the dCP mode is mainly due to the S2, and that of the continuum near $k=\pi$ is mainly due to the S3. The contributions from these string solutions increase as the magnetic field decreases as shown by solid symbols in Fig. 2 (a). By taking them into account, more than 80% of the total spectral weight in $S^{+-}(k, \omega)$ is explained in a wide range of S^z in $L=320$ [27].

As for n -string solutions ($n \geq 2$) in $S^{zz}(k, \omega)$, we found that a large spectral weight is carried by S2 with $2\psi_s$ in low fields. As shown by solid squares in Fig. 2 (b), the decrease of $S^{zz}(k, \omega)$ of up to $2\psi 2\psi^*$ excitations in the small S^z regime (open squares in Fig. 2 (b)) is almost compensated for by the S2, and more than 90% of the total spectral weight in $S^{zz}(k, \omega)$ is explained in a wide range of S^z in $L=320$ [27]. These string solutions are relevant to the continuum near $k=\pi$ in low fields.

Figure 3 (a) shows behaviors of dynamical structure factors in magnetic fields in $L=320$, where we took into account excitations of up to $2\psi 2\psi^*$ and the above-described string solutions. Hereafter, we use these excitations to calculate dynamical structure factors. In $S^{+-}(k, \omega)$, there are three sets of dominant continua as shown in the top row of Fig. 3 (a). The high-energy continuum ($\omega/J \gtrsim 2$), which is mainly due to S2, goes up to higher energies as the magnetic field increases, separated from the low-energy continua. Although this continuum has been observed in the high-field regime by numeri-

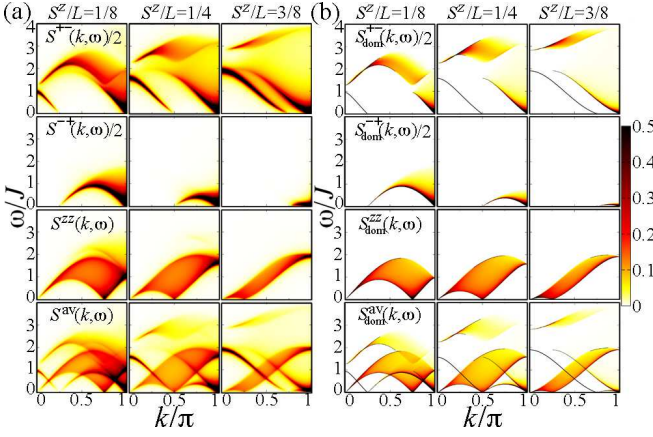


FIG. 3: (a) $S^{+-}(k, \omega)/2$, $S^{-+}(k, \omega)/2$, $S^{zz}(k, \omega)$ and $S^{av}(k, \omega)$ (from above) at $S^z/L=1/8$, $1/4$ and $3/8$ (from the left) in $L=320$. The data are broadened in a Lorentzian form with $\text{FWHM}=0.08J$. (b) Same as (a) but those of dynamically dominant excitations in $L=2240$ with the product ansatz.

cal calculations [9, 19, 20], the relation to the S2 has not been clarified. Near the saturation field, these string solutions reduce to bound states of two overturned spins from the ferromagnetic state [1, 9] with the excitation energy given by $\omega(k) = \frac{J}{2}(3 - \cos k) + H$. As for $S^{-+}(k, \omega)$ and $S^{zz}(k, \omega)$, there is basically one continuum for each correlation as shown in the second and third rows of Fig. 3 (a), respectively. The additional high-energy continuum at $S^z/L=1/8$ in $S^{zz}(k, \omega)$ near $k=\pi$ mainly comes from S2.

From many excitations considered above, we extract dynamically dominant excitations of $O(L^2)$ states which characterize the behaviors of Fig. 3 (a). Then, the product ansatz [11]: $S^{\alpha\alpha}(k, \omega) = M^{\alpha\alpha}(k, \omega)D(k, \omega)$ with $D(k, \epsilon_k^i) = 2/(\epsilon_k^{i+1} - \epsilon_k^{i-1})$ can be applied. Here, in energy regions where there is more than one sequence of states, we took the one with the largest spectral weight. Hereafter, we denote $S^{\alpha\alpha}(k, \omega)$ of the dynamically dominant excitations as $S_{\text{dom}}^{\alpha\alpha}(k, \omega)$ for $\alpha = -, +$ and z . Their contributions to sum rules in $L=2240$ are shown in Fig. 2 (c).

The top row of Fig. 3 (b) shows $S_{\text{dom}}^{+-}(k, \omega)$. The high-energy continuum near $\omega/J \gtrsim 2$ is due to S2 with $1\psi_s$ as in Fig. 1 (f-1), which can be regarded as a part of the above-mentioned S2 with $\psi_s\psi_s^*$. The low-energy continuum near $k=\pi$ comes from $2\psi^*$ excitations where two ψ^* s are located on opposite sides of the filled region of $\{I_j\}$ from each other as in Fig. 1 (d). The low-energy mode near $k=0$ is due to excitations with one ψ^* in the right empty region of $\{I_j\}$ for $0 \leq k \leq \pi$ as in Fig. 1 (e). This mode has been mentioned in the literature [9, 10, 18, 19, 20].

The dynamically dominant excitations for $S^{-+}(k, \omega)$ and $S^{zz}(k, \omega)$ are known as 2ψ and $\psi\psi^*$ excitations as in Fig. 1 (c) and (b), respectively [10, 11]. The results are shown in the second and third rows of Fig. 3 (b).

Noting that 2ψ , $\psi\psi^*$ and $2\psi^*$ excitations are dynamically dominant in $S^{-+}(k, \omega)$, $S^{zz}(k, \omega)$ and $S^{+-}(k, \omega)$

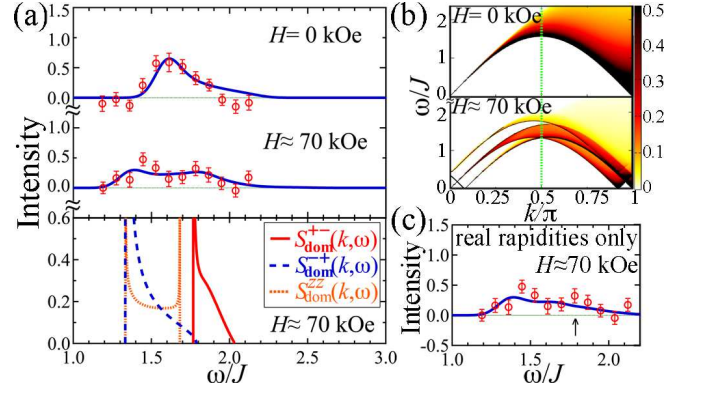


FIG. 4: Comparison with experimental results on $\text{CuCl}_2 \cdot 2\text{N}(\text{C}_5\text{D}_5)$. (a) Solid lines in upper two panels are the present results of $S^{av}(k, \omega)$ at $k=\pi/2$ in $L=320$. The data are broadened in a gaussian form with $\text{FWHM} \approx 0.17J$. Open symbols are experimental results in Ref. [28]. The height is rescaled after subtracting the background ($=180$ counts). The lowest panel shows lineshapes of $S_{\text{dom}}^{\alpha\alpha}(k, \omega)$ ($\alpha = -, +$ and z) at $k=\pi/2$ in $L=2240$. (b) $S_{\text{dom}}^{\alpha\alpha}(k, \omega)$ in $L=2240$. (c) Same as the middle panel of (a) except that the solid line is obtained from solutions with real rapidities only. The arrow indicates the high-energy peak observed in the experiment [28].

and that these excitations have $S^z = +1, 0$ and -1 , respectively, we can naturally assign $S^z = +1/2$ and $-1/2$ to ψ and ψ^* , respectively. Also, noting that excitations of S2 with $\psi_s\psi_s^*$ and those with $2\psi_s$ have large weights in $S^{+-}(k, \omega)$ and $S^{zz}(k, \omega)$ and that these excitations have $S^z = -1$ and 0 , respectively, we can naturally interpret the quasiparticle representing the 2-string (Fig. 1 (f-2)) as a bound state of two ψ^* s which carries $S^z = -1$. This assignment is also applicable to 4-spinon states of $S^{-+}(k, \omega)$ in zero field which have four spinons and a 2-string. The $1\psi^*$ mode near $k=0$ in $S^{+-}(k, \omega)$ can also be regarded as the most dominant part of a $2\psi^*$ continuum where both ψ^* s are located in the right empty region of $\{I_j\}$ (Fig. 1 (e) as compared with (d)) for $0 \leq k \leq \pi$. But, since the spectral weight in this continuum is very small except the $1\psi^*$ mode, the ψ^* in this mode practically behaves as a quasiparticle carrying $S^z = -1$, which reduces to a magnon carrying $S^z = -1$ above the saturation field.

To confirm the relevance to real materials, we compare the present results with available experimental data on quasi-one-dimensional materials which can be effectively regarded as spin-1/2 antiferromagnetic Heisenberg chains. In inelastic neutron scattering experiments, a quantity proportional to $S^{av}(k, \omega)$ is observed. Here, we define $S^{av}(k, \omega) \equiv [S^{-+}(k, \omega) + S^{+-}(k, \omega) + 4S^{zz}(k, \omega)]/6$. The fourth row of Fig. 3 shows the results of $S^{av}(k, \omega)$ and $S_{\text{dom}}^{av}(k, \omega)$, where $S_{\text{dom}}^{av}(k, \omega)$ denotes $S^{av}(k, \omega)$ of the dynamically dominant excitations.

In Fig. 4 (a), we compare the present results with experimental results on $\text{CuCl}_2 \cdot 2\text{N}(\text{C}_5\text{D}_5)$ (CPC) [28]. We broadened the numerical results of $S^{av}(k, \omega)$ in a gaus-

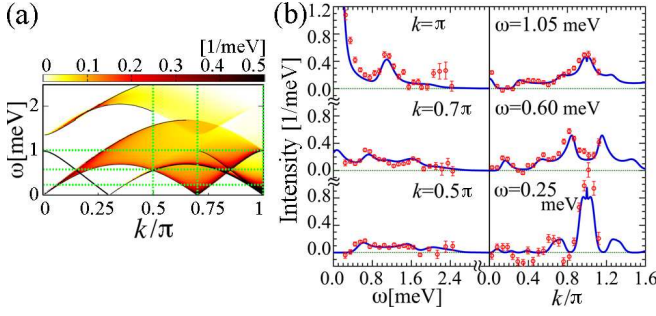


FIG. 5: Comparison with experimental results on $\text{Cu}(\text{C}_4\text{H}_4\text{N}_2)(\text{NO}_3)_2$. (a) $S^{\text{av}}_{\text{dom}}(k, \omega)$ at $S^z/L=0.15$ in $L=2240$. (b) Solid blue lines denote $S^{\text{av}}(k, \omega)$ in $L=320$ along green dotted lines in (a). The data are broadened in a gaussian form with standard deviation $\sigma=0.1$ meV. Open symbols are experimental results of intensity at $H=8.7$ T in Ref. [8]. Here, we subtracted the background equal to that of $H=0$ [8].

sian form in zero field, and rescaled the experimental data in Ref. [28] after subtracting the background. Using the same broadening and rescaling parameters, we calculated $S^{\text{av}}(k, \omega)$ at $H \approx 70$ kOe and compared it with experimental results, where we used g -factor $g=2.08$ and $J=27.32$ K [29]. The positions and intensities of the two peaks at $H=70$ kOe observed in the experiment are reasonably reproduced by the present results as shown in the middle panel of Fig. 4 (a). The high- and low-energy peaks are mainly due to S2 in $S^{+-}(k, \omega)$ and 2ψ excitations in $S^{-+}(k, \omega)$, respectively, as shown in the lowest panels of Fig. 4 (a) and (b). For comparison, the results of solutions with real rapidities only are shown in Fig. 4 (c). Obviously, the spectral weight at the high-energy peak is missing, if n -string solutions ($n \geq 2$) are neglected.

Figure 5 (b) shows comparisons with experimental results on $\text{Cu}(\text{C}_4\text{H}_4\text{N}_2)(\text{NO}_3)_2$ (CuPzN) [8] along scans denoted by green dotted lines in Fig. 5 (a). The present results reasonably agree with the experimental results. Figure 5 (a) is plotted so that it can be easily compared with Fig. 4 (a) in Ref. [8]. A signature of the high-energy continuum originating from the 2-string solutions was observed near $k \approx 0.3\pi$ and $\omega \approx 2$ meV in the experiment [8].

Signatures of the 2-string solutions in an anisotropic two-dimensional system will be shown elsewhere [30].

In summary, we have investigated dynamical properties of the spin-1/2 antiferromagnetic Heisenberg chain in magnetic fields, using Bethe-ansatz solutions. We found that string solutions with a 2-string have considerable spectral weight in $S^{+-}(k, \omega)$, and can be regarded as dynamically dominant excitations of $S^{+-}(k, \omega)$. This indicates that not only ψ and ψ^* but also the quasiparticle representing the 2-string plays an important role for the dynamical properties in magnetic fields. The continuum of these solutions continuously connects the dCP mode in

the zero-field limit and that of bound states of overturned spins from the ferromagnetic state [1] near the saturation field. Another finding is that $2\psi^*$ excitations are identified as the dominant excitations of $S^{+-}(k, \omega)$ near $k=\pi$ in the low-energy regime, which leads to a natural interpretation of ψ and ψ^* as quasiparticles in magnetic fields carrying $S^z=+1/2$ and $-1/2$, respectively. Comparisons with available experimental results reasonably support the relevance to real materials. For clear identification of dynamically dominant excitations, further experiments in higher fields at high energies are desired. Behaviors shown in this Letter are expected to be more or less true for general spin-1/2 XXZ chains in magnetic fields.

Acknowledgements - I am grateful to L. Balents, M. Shiroishi, M. Arikawa, O.A. Starykh, R. Coldea, M. Takahashi and A. Tanaka for discussions, helpful comments and suggestions. This work was supported by KAKENHI 20740206 and 20046015, and World Premier International Research Center Initiative, MEXT, Japan.

-
- [1] H. Bethe, Z. Phys. **71**, 205 (1931).
 - [2] L. D. Faddeev *et al.*, Phys. Lett. A **85**, 375 (1981).
 - [3] F. D. M. Haldane, Phys. Rev. Lett. **66**, 1529 (1991).
 - [4] D. A. Tennant *et al.*, Phys. Rev. B **52**, 13368 (1995).
 - [5] D. C. Dender *et al.*, Phys. Rev. B **53**, 2583 (1996).
 - [6] P. R. Hammar *et al.*, Phys. Rev. B **59**, 1008 (1999).
 - [7] N. Ishimaru, and H. Shiba, Prog. Theor. Phys. **57**, 1862 (1977); *ibid.* **64**, 479 (1980).
 - [8] M. B. Stone *et al.*, Phys. Rev. Lett. **91**, 037205 (2003).
 - [9] G. Müller *et al.*, Phys. Rev. B **24**, 1429 (1981).
 - [10] M. Karbach *et al.*, Phys. Rev. B **66**, 054405 (2002).
 - [11] M. Karbach *et al.*, Phys. Rev. B **62**, 14871 (2000).
 - [12] A. Fledderjohann *et al.*, Phys. Rev. B **54**, 7168 (1996).
 - [13] J. -S. Caux *et al.*, Phys. Rev. Lett. **95**, 077201 (2005).
 - [14] R. G. Pereira *et al.*, Phys. Rev. Lett. **96**, 257202 (2006).
 - [15] J. Sato *et al.*, J. Phys. Soc. Jpn. **73**, 3008 (2004).
 - [16] J. -S. Caux *et al.*, J. Stat. Mech. P09003 (2005).
 - [17] D. Biegel *et al.*, J. Phys. A: Math. Gen. **36** 5361 (2003).
 - [18] D. Biegel *et al.*, Europhys. Lett. **59**, 882 (2002).
 - [19] S. Nishimoto *et al.*, Int. J. Mod. Phys. B **21**, 2262 (2007).
 - [20] K. Lefmann *et al.*, Phys. Rev. B **54**, 6340 (1996).
 - [21] R. B. Griffiths, Phys. Rev. **133**, A768 (1964).
 - [22] M. Takahashi, Prog. Theor. Phys. **46**, 401 (1971).
 - [23] R. Hagemans *et al.*, AIP Conf. Proc. **846**, 245 (2006).
 - [24] N. Kitanine *et al.*, Nucl. Phys. B **554**, 647 (1999).
 - [25] The total spectral weights of $S^{\alpha\alpha}(k, \omega)$ ($\alpha=-, +$ and z) are $L-M$, M and $L/4-(S^z)^2/L$, respectively [13, 16].
 - [26] J. des Cloizeaux *et al.*, Phys. Rev. **128**, 2131 (1962).
 - [27] Judging from small size-dependence in $L \lesssim 320$ for Fig. 2 (a,b), we believe the physics will hold for larger systems.
 - [28] I. U. Heilmann *et al.*, Phys. Rev. B **18**, 3530 (1978).
 - [29] J. A. Chakhalian *et al.*, Phys. Rev. Lett. **91**, 027202 (2003).
 - [30] M. Kohno (unpublished).